Vietnam Journal of Catalysis and Adsorption
Tap chí xúc tác và hấp phụ Việt Nam

http://chemeng.hust.edu.vn/jca/

Synthesis and characterizations of titanium nitride nanofibers prepared using nitridation method

Mai Thi Tuyet Trinh,[1] Le Xuan Hung,[2] Le Thi Thanh Hiep,[3] Le Thi Ngoc Loan[1]*

[1] *Department of Physics, Faculty of Natural Sciences, Quy Nhon University, Quy Nhon city, VIETNAM*
[2] *Institute of Research and Development, Duy Tan University, Da Nang city, VIETNAM*
[3] *Office of Scientific Research and Technology, Duy Tan University, Da Nang city, VIETNAM*
**Email: lethingocloan@qnu.edu.vn*

ARTICLE INFO

Received: 05/6/2020
Accepted: 30/6/2020

Keywords:
Titanium nitride nanofibers, solar water evaporation, plasmonic materials, nano-heater sources

ABSTRACT

In this paper, titanium nitride nanofibers (TiN NFs) were successfully synthesized by nitridation of TiO_2 nanofibers, in which the TiO_2 nanofibers were prepared by using electrospinning method. The XRD patterns and Raman spectra indicate that transformation of TiO_2 into TiN crystalline structure was succeeded at 900°C in ammonia at flow rate of 800 sccm in 60 mins. The SEM images show no significant change in morphology, however, surface of the sample annealed at 900°C becomes rougher compared to that of TiO_2 nanofibers. The UV-vis absorption spectrum of TiN illustrates a strong and broad absorption peak at 530 nm which covers entire visible part of the solar spectrum. The as-synthesized samples were used to test solar water evaporation and the results indicate that TiN nanofibers are great nano-heater sources to enhance water evaporation performance.

Introduction

Titanium nitride (TiN) has been widely used as a decorative, coating, and cutting material due to its superior hardness, excellent thermal stability, high melting point and corrosion resistance [1][2]. Moreover, TiN exhibits high electric conductivity, high transmittance and good chemical stability [3, 4]. In recent years, TiN nanostructures have attracted much attention for various applications in the fields of optoelectric devices [4], solar cells [5], supercapacitors [6], and batteries [7], electrocatalysts [6]. Hence, TiN has been become a promising plasmonic material because it not only shows good plasmonic performance but also offers excellent mechanical strength and durability, compatibility with CMOS technology and cost effectiveness, which overcomes limitation of traditional plasmonic metals like gold and silver [8, 9]. In addition, TiN provided a high and broadband absorption efficiency and had strong surface plasmon resonance in the visible and near infrared region [10-12]. Due to the surface plasmon resonance effect, light is concentrated into nanoscale volumes at the interface of a dielectric, providing intense electromagnetic field localization and improving scattering. As a result, TiN becomes a potential candidate for plasmonic applications, i.e., solar energy conversion [13], sensing [14], catalysis [15]. Noticeably, TiN is one of the best material choice for emerging thermoplasmonics due to enhanced performance of sunlight absorption, using for many applications in high-temperature catalysis [16], solar heat transducers [17] and, especially, solar water evaporation [18, 19].

Since carbon nanotubes were discovered [20], synthesis of one dimensional (1D) has drawn tremendous attention due to their high aspect ratio,

unique-size and dimensionality-dependent electrical, optical, chemical and mechanical properties. Likewise, efforts for the growth of TiN 1D structures have been reported by several groups for biological, electronic and, especially, photonic applications. Kim et al. has prepared titanium nitride nanofibers (TiN NFs) as a catalyst supported for proton exchange membrane fuel cell by using a combination of electrospinning and two-step calcination techniques [6]. Lu and his co-workers grew TiN nanowires on the carbon cloth via a seed-assisted hydrothermal method following by annealing step in ammonia [21], whilst Yi Chen group reported on TiN nanowires preparation through a chloride-assisted carbon thermal reduction route [22]. Hierarchical TiN nanotube mesh was prepared by calcining TiO_2 nanotube mesh (TONM) in NH_3 flow where the TONM is fabricated by electrochemical anodic oxidation of Ti mesh [19]. Titanium nitride nanorod arrays were prepared as surface-enhanced Raman scattering (SERS) substrates using glancing angle deposition in a magnetron sputtering system [14]. Although lots of effort have been made for TiN synthesis, strategies for a scalable and inexpensive pathway to grow one-dimensional nanostructured TiN is still limited. In this work, we present a low-cost, simple and scalable method to synthesize TiN NFs. Interestingly, the UV-vis absorption showed a strong and broad surface plasmon resonance peak lying in the visible region of the solar spectrum. This results in a high solar-heat conversion efficiency, thus, enhancing water evaporation under sunlight irradiation.

Experimental

Chemicals

All chemicals were purchased and utilized without further purification: poly(vinylpyrrolidone) (PVP) (wt 360000, Sigma–Aldrich Co., Ltd), ethanol (C_2H_5OH, 99.8%), acetic acid (CH_3COOH, 99%), titanium tetraisopropoxide [$Ti(OiPr)_4$; 97%, Sigma-Aldrich Co., Ltd], distilled water (18.4 MΩ/cm), pure nitrogen and ammonia gas (N_2 &NH_3, ≥99,9%) .

TiO_2 nanofibers preparation

The TiO_2 nanofibers (TiO_2 NFs) were synthesized using electro-spinning method similar to previous report [23]. Briefly, 0.4 grams of poly(vinylpyrrolidone) was dissolved in 8 mL of ethanol and stirred for 2 h. Next, 6 mL of titanium tetraisopropoxide and 4 mL of acetic acid were added to the as-prepared solution and stirred for 60 mins at room temperature to obtain a sufficiently viscous solution for electro-spinning. Following step was to inject the precursor solution into a 5-ml syringe mounted on the syringe pump and fed into a metal needle. The precursor was then electro-spun by applying a high DC voltage of 10 kV across a distance of 10 cm toward the grounded collector. Noticeably, the precursor was constantly added by the syringe pump at a rate of 0.05 mL/h. A silicon substrate (5 × 5 cm) was placed on the grounded collector for collection of nanofibers. After 2 hours of collection, the composite Ti(OiPr)4/PVP nanofibers on the Si substrate were collected and dried in air ambient for 3h at 500°C to form the TiO_2 NFs.

TiN nanofibers synthesis

The obtained TiO_2 NFs in the previous step were used as precursor to synthesize TiN NFs by thermal annealing in ammonia at a temperature of 900°C. Initially, TiO_2 NFs were loaded in a ceramic boat and placed in a tube oven. One end of the tube was connected with a nitrogen and ammonia gas cylinder through two mass flow controllers MFC1 and MFC2, respectively. The other end of the tube was connected with a vacuum pump. Before heating up, the chamber of the oven was evacuated to reach a pressure of approx. 10^{-3} Torr. The oven was then pre-heated to 250°C and purged with nitrogen gas several times in 30 mins to remove contaminants. After that, the temperature in the chamber was increased to 900°C at the ramping speed of 5°C/min, then closed the MFC1 and opened MFC2 to flow ammonia gas into the chamber at a flow rate of 800 sccm for 2h hours. Finally, when the oven was naturally cooled down below 100°C, closed MFC2 and opened MFC1 before collecting the samples.

Characterizations

The morphology, crystalline structure of the samples were examined by field–emission scanning electron microscopy (FE–SEM; Hitachi S4800), X–ray diffraction (XRD, D8 Advance Eco, Bruker). The optical absorption spectra were obtained from the JASCO V-750 UV-Vis Spectrophotometer. Raman measurements were done using the XploRa Plus microscpe, Horiba Jobin, laser 532 nm and integration time of 10s.

For water evaporation testing, 20 mg of each sample annealed at 900°C (hereafter denoted as sample@900), and as-synthesized TiO_2 NFs was added into 40 mL water contained in a 100 mL-glass beaker (denoted as S2 and S1 solution, respectively) and sonicated for 15 mins to evenly distribute TiN NFs in water and avoid aggregation. The beaker was then placed on an electronic balance for determination of vaporized weights during illumination. A tungsten

filament light bulb (40W) was used to expose the above solution.

Results and discussion

Structural analysis

The X-ray diffraction (XRD) spectra exhibit crystal phase transformation of these materials during nitridation process. Fig. 2 shows XRD patterns of the as-synthesized TiO_2 NFs and the sample annealed in ammonia at 900°C (denoted as sample@900). The XRD pattern of TiO_2 NFs, seen in Fig. 1a, indicates a mixture of anatase and rutile phase (according to the JCPDS card No. 84-1286 and No. 75- 1753) in which the TiO_2 anatase phase is dominant (by comparing peak area of the strongest peak A(101) versus R(110)). Fig. 1b illustrates crystal structure transformation when annealing TiO_2 NFs in ammonia at 900°C.

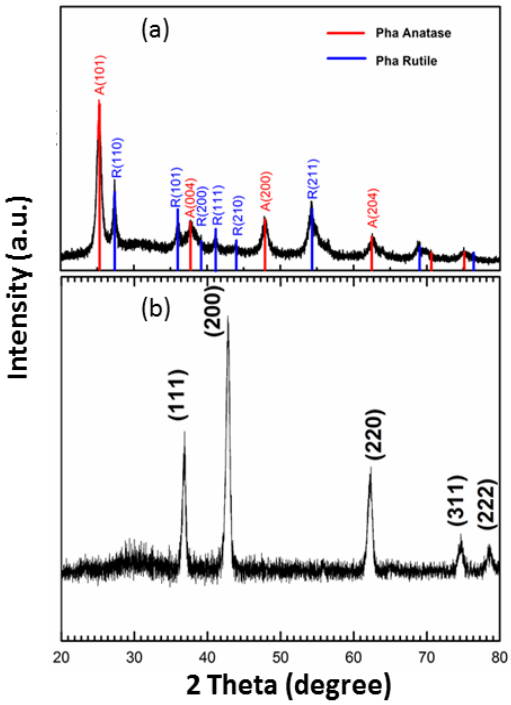

Figure 2: XRD patterns of the as-synthesized TiO_2 NFs (a) and the sample annealed at 900°C in amonia (b)

The result shows there are five strong X-ray diffraction peaks at 2θ of 36.3°; 42.2°; 61.6°; 73.8° and 77.6°, which respectively corresponded to (111), (200), (220), (311) and (222) lattice planes of face centered cubic (FCC) structure of TiN (according to the JCPDS card, No.38-1420). These five peaks are strong and sharp suggesting that the sample@900°C is well-crystallized. No other peaks can be detected implying that a complete transformation of TiO_2 into TiN crystalline structure can be achieved at 900°C in ammonia for 60 mins. The strongest diffraction peak is indexed to the cubic TiN oriented in (200) plane, which might refer to the growth of TiN nanofibers.

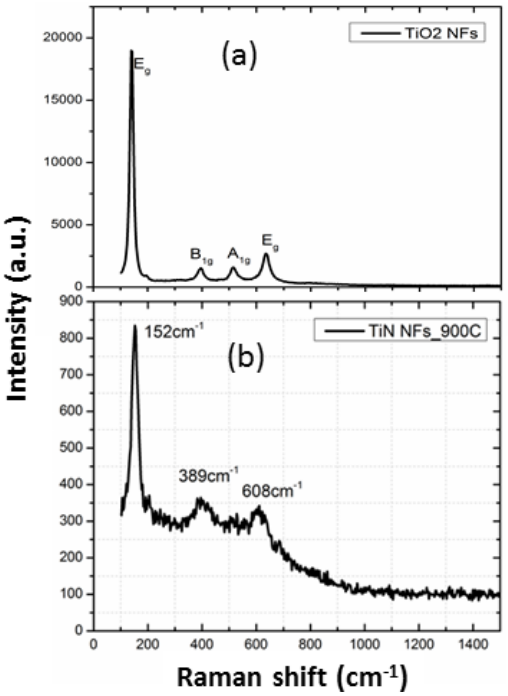

Figure 3: Raman spectra of as-synthesized TiO_2 (Fig. 3a) with four typical Raman active modes of anatase phase and TiN (Fig. 3b) with two characteristics of acoustic range and optic range.

Composition and structure of the as-synthesized materials were further characterized by using Raman spectroscopy, a powerful and non-destructive method in order to study the chemical structure and phase of materials. According to report of Ohsaka [24], the typical TiO_2 anatase single crystal has six vibration modes at Raman shift of 144 cm^{-1} (Eg), 197 cm^{-1} (Eg), 399 cm^{-1} (B1g), 513 cm^{-1} (A1g), 519 cm^{-1} (B1g), and 639 cm^{-1} (Eg). Fig. 3a demonstrates Raman spectrum of the as-synthesized TiO_2 in the range of 100 -1100 cm^{-1}, illustrating four strong peaks at 140 cm^{-1}, 395 cm^{-1}; 513 cm^{-1}, and 637 cm^{-1}, which corresponds to four Raman active modes of E_g, B_{1g}, A_{1g}, and E_g, respectively; no Raman peak of TiO_2 rutile phase can be observed too. These Raman characteristics show the dominant anatase phase of the as-prepared TiO_2, which is in a good agreement with the XRD patterns as shown in Fig. 2a. Furthermore, due to the reaction of TiO_2 with NH_3 gas, oxygen atoms in the TiO_2 lattice were replaced by nitrogen atoms to form TiN crystalline. The Raman peaks at 152 cm^{-1}, 389 cm^{-1} and 608 cm^{-1} in Fig. 3b are ascribed to transverse acoustic (TA), longitudinal acoustic (LA) and transverse optical (TO) modes of the cubic TiN crystal, respectively[25].

The XRD and Raman characterizations indicate that the TiO_2 have been successfully converted into TiN

crystalline structure by annealing in ammonia at 900°C for 60 mins.

Morphology characterization

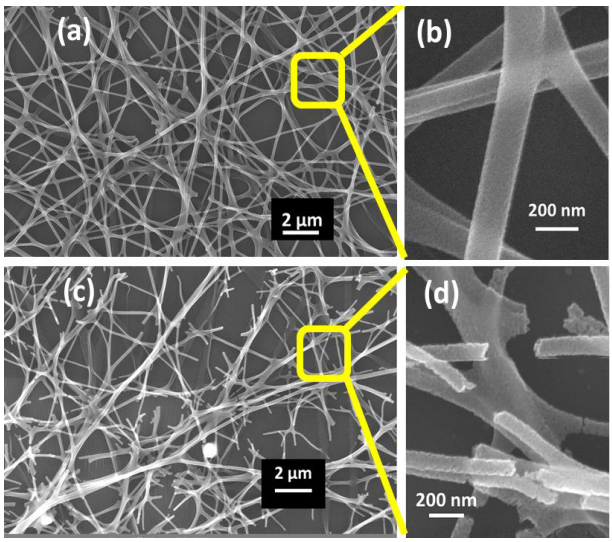

Figure 4: SEM images of TiO_2 NFs (a) and sample@900 (c) the surface of TiO_2 is smooth (b) compared to that of sample@900

Morphology of the synthesized samples were characterized using scanning electron microscopy (SEM). Fig. 4a shows the size of TiO_2 NFs are in the 100-200 nm diameter range and up to few micrometer in length. Fig. 4c demonstrates there is no significant chance in morphology between the synthesized-TiO_2 and –the sample@900; nonetheless, part of TiN NFs were broken due to high temperature annealing process. Interestingly, the surface of the TiN NFs becomes rougher and more open (Fig. 4d) compared to that of TiO_2 NWs (Fig. 4b), which is attributed to calcination process and nitrogen gas release during the reaction of TiO_2 with ammonia to form TiN [26], the reaction can be described as below:

$$6TiO_2 + 8NH_3 \rightarrow 6TiN + 12H_2O + N_2\uparrow$$

The roughness could increase the specific surface area of TiN NFs, which might be interesting for light absorption, sensing and catalysis performance of this material.

UV-vis absorption

Due to its large band gap, titanium dioxide nanofibers exhibit intrinsically strong absorption of ultraviolet (UV) light. Using Tauc method to determine optical band gap insemiconductors, the band gap of the as-synthesized TiO_2 NFs is 3.15 eV (Fig. 5a), this is in good agreement with other reports [27]. In contrast, the absorption characteristic of a semiconduction in Fig.5b is completely vanished, instead, TiN NFs has a strong absorption peak at 530 nm, which is attributed to plasmon resonance effect.

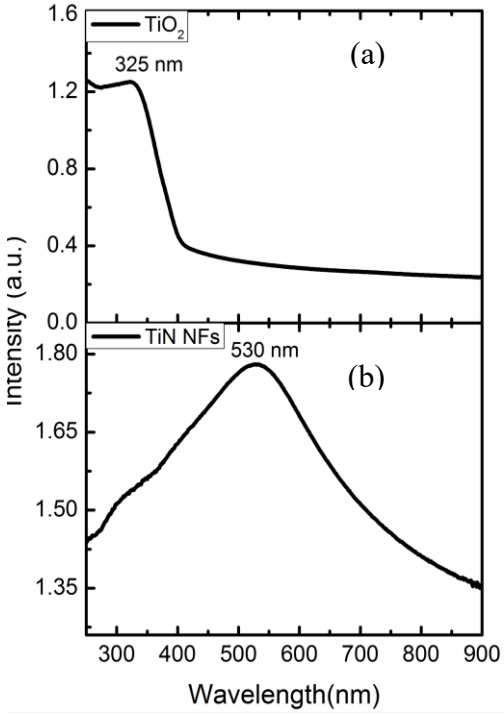

Figure 5: UV-vis absorption spectrum of TiO_2 NFs (a) and of TiN NFs (b)

Noticeably, this peak lies in the visible region which is broad and entirely covers the solar spectrum. Modeling TiN absorption spectrum using Gaussian function, the result shows full with half maximum (FWHM) of 265 nm. This value is quite large compared to traditional plasmonic materials like gold or silver. Furthermore, the plasmon resonance peak of TiN NFs is blue-shifted, compared to previous works [10], this requires further studies to understand plasmonic behavior of the as-prepared TiN using nitridation method.

Solar water evaporation measurements

The blue-triangular line in Fig. 6 shows weight loss of S2 due to evaporation process, which is much higher compared to that of S1 (red-dotted line) and pure water (denoted as solution S0, black-squared line). Under continued illumination using simulated solar light of 38k lux (approximately 300 W/m^2 or one-third Sun), after one hour, the evaporation rate of solution S2; S1 and S0 acquired about 0.31; 0.20 and 0.17 kg h^{-1} m^{-2}, respectively. The evaporation rate of S1 is slightly higher than S0 due to its better absorption of sunlight, whereas the outstanding rate of S2 is resulted from the plasmon resonance (PR) effect. Hence, this strong and broad PR peak lies in the visible region and covers the solar spectrum, the as-synthesized TiN NFs become an

active agent to improve the solar absorption efficiency and generate heat, thus, increase the evaporation rate of S2 solution.

The enhancement of water evaporation in this case can be interpreted by using the model proposed by Neumann [28] as follows: TiN NFs strongly absorbs sunlight to generate an enhanced electric field on TiN NFs' surface and its vicinity. This electric field locally heats up a layer of water surrounding the surface of the nanofibers and vaporizes the water. Fig. 7 illustrates the vaporization enhancement process enabled by TiN NFs

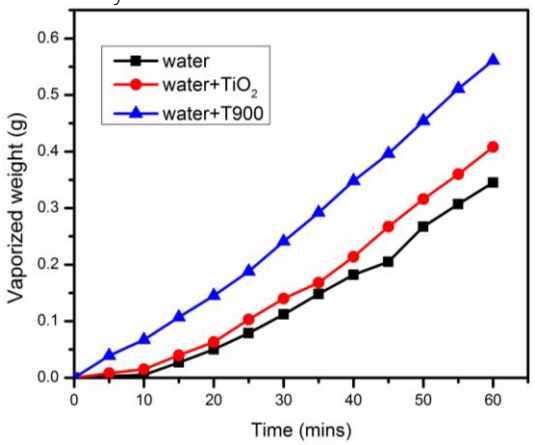

Figure 6: Comparison of water evaporation under simulated sunlight illuminace of pure water (black-squared line, S0), water +TiO_2 solution (red-dotted line, S1) and water +TiN solution (blue-triangular line, S2)

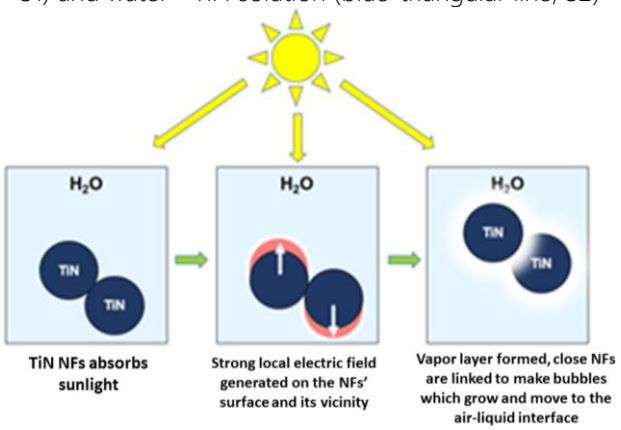

Figure 7: schematic representation of evaporation process demonstrates how TiN NFs absorbs sunlight and locally heats water

If the illumination continues, this vapor layer will grow larger, in addition, the closed TiN NFs in the solution could aggregate and create bubbles. These bubbles will develop in volume and eventually move to the surface of the liquid. At the air-liquid interface, the vapor is released and the TiN NFs return to the liquid to perform another vaporization cycles until the illumination stops. Outstandingly, this vaporization process occurs locally and differentiates from traditional vaporization process where the entire liquid volume requires to be heated, thus, consumes much more energy to vaporize similar amount of water.

Conclusion

Titanium nitride nanofibers were successfully synthesized using a two-step process: electrospinning followed by nitridation. There is no significant change in morphology between TiN NFs and TiO_2 NFs except for the surface roughness. The UV-vis absorption spectra show significant change from TiO_2 to TiN where TiN NFs has a strong and broad absorption peak centered at 530 nm, covering entirely the visible part of the solar spectrum. This is attributed to the surface plasmon resonance effect. As a result, TiN NFs enhances sunlight absorption efficiency, thus, increases evaporation rate, up to 0.31, in comparision with TiO_2 solution and water, about 0.20 and 0.17 kg h^{-1} m^{-2} respectively.

Acknowledgments

This research is funded by the Ministry of Education and Training (MOET) under grant number B2018-DQN-06.

References

1. Aronson AJ, Chen D, Class WH. Preparation of titanium nitride by a pulsed d.c. magnetron reactive deposition techniques using the moving mode of deposition. Thin Solid Films 72(3) (1980)535-540. https://doi.org/10.1016/0040-6090(80)90544-1
2. Komiya S, Umezu N, Hayashi C. Titanium nitride film as a protective coating for a vacuum deposition chamber. Thin Solid Films. 1979;63(2):341-346. https://doi.org/10.1016/0040-6090(79)90038-5
3. Nakayama T, Wake H, Ozawa K, Kodama H, Nakamura N, Matsunaga T. Use of a titanium nitride for electrochemical inactivation of marine bacteria. Environ Sci Technol. 1998;32(6):798-801. https://doi.org/10.1021/es970578h
4. Li H, Pan W, Zhang W, Huang S, Wu H. TiN nanofibers: A new material with high conductivity and transmittance for transparent conductive electrodes. Adv Funct Mater. 2013;23(2):209-214. https://doi.org/10.1002/adfm.201200996
5. Xu H, Zhang X, Zhang C, et al. Nanostructured titanium nitride/PEDOT:PSS composite films as counter electrodes of dye-sensitized solar cells. ACS Appl Mater Interfaces. 2012;4(2):1087-1092. https://doi.org/10.1021/am201720p

6. Kim H, Cho MK, Kwon JA, et al. Highly efficient and durable TiN nanofiber electrocatalyst supports. https://doi.org/10.1039/c5nr04082e
7. Zhong Y, Xia XH, Shi F, Zhan JY, Tu JP, Fan HJ. Transition metal carbides and nitrides in energy storage and conversion. Adv Sci. 2015;3(5). https://doi.org/10.1002/advs.201500286
8. Naik G V., Shalaev VM, Boltasseva A. Alternative plasmonic materials: Beyond gold and silver. Adv Mater. 2013;25(24):3264-3294. https://doi.org/10.1002/adma.201205076
9. Khurgin JB, Boltasseva A. Reflecting upon the losses in plasmonics and metamaterials. MRS Bull. 2012;37(08):768-779. https://doi.org/10.1557/mrs.2012.173
10. Guler U, Suslov S, Kildishev A V., Boltasseva A, Shalaev VM. Colloidal Plasmonic Titanium Nitride Nanoparticles: Properties and Applications. Nanophotonics. 2015;4(1):269-276. https://doi.org/10.1515/nanoph-2015-0017
11. Li W, Guler U, Kinsey N, et al. Refractory plasmonics with titanium nitride: Broadband. Adv Mater. 2014;26(47):7959-7965. https://doi.org/10.1002/adma.201401874
12. Jacob Z, Smolyaninov II, Narimanov EE. Broadband Purcell effect: Radiative decay engineering with metamaterials. Appl Phys Lett. 2012;100(18):534-537. https://doi.org/10.1063/1.4710548
13. Khalifa AE, Swillam MA. Plasmonic silicon solar cells using titanium nitride: a comparative study. J Nanophotonics. 2014;8(1):084098. https://doi.org/10.1117/1.jnp.8.084098
14. Jen YJ, Lin MJ, Cheang HL, Chan TL. Obliquely deposited titanium nitride nanorod arrays as surface-enhanced raman scattering substrates. Sensors (Switzerland). 2019;19(21). https://doi.org/10.3390/s19214765
15. Shin H, Kim H Il, Chung DY, et al. Scaffold-like titanium nitride nanotubes with a highly conductive porous architecture as a nanoparticle catalyst support for oxygen reduction. ACS Catal. 2016;6(6):3914-3920. https://doi.org/10.1021/acscatal.6b00384
16. Naldoni A, Kudyshev ZA, Mascaretti L, et al. Solar thermoplasmonic nanofurnace for high-temperature heterogeneous catalysis. Nano Lett. 2020;20(5):3663-3672. https://doi.org/10.1021/acs.nanolett.0c00594
17. Ishii S, Sugavaneshwar RP, Nagao T. Titanium Nitride Nanoparticles as Plasmonic Solar Heat Transducers. J Phys Chem C. 2016;120(4):2343-2348. https://doi.org/10.1021/acs.jpcc.5b09604
18. Kaur M, Ishii S, Shinde SL, Nagao T. All-ceramic solar-driven water purifier based on anodized aluminum oxide and plasmonic titanium nitride. Opt InfoBase Conf Pap. 2018;Part F125-:1-8. https://doi.org/10.1002/adsu.201800112
19. Ren P, Yang X. Synthesis and Photo-Thermal Conversion Properties of Hierarchical Titanium Nitride Nanotube Mesh for Solar Water Evaporation. Sol RRL. 2018;2(4):1-7. https://doi.org/10.1002/solr.201700233
20. Iijima, S. (1991) Synthesis of Carbon Nanotubes. Nature, 354, 56-58. http://dx.doi.org/10.1038/354056a0.
21. Lu X, Wang G, Zhai T, et al. Stabilized TiN nanowire arrays for high-performance and flexible supercapacitors. Nano Lett. 2012;12(10):5376-5381. https://doi.org/10.1021/nl302761z
22. Hu Y, Huo K, Ma Y, et al. Synthesis and field emission characterization of titanium nitride nanowires. J Nanosci Nanotechnol. 2007;7(8):2922-2926. https://doi.org/10.1166/jnn.2007.686
23. Nguyen VN, Nguyen MV, Nguyen THT, et al. Surface-modified titanium dioxide nanofibers with gold nanoparticles for enhanced photoelectrochemical water splitting. Catalysts. 2020;10(2):1-11. https://doi.org/10.3390/catal10020261
24. Ohsaka T, Izumi F, Fujiki Y. Raman spectrum of anatase, TiO2. J Raman Spectrosc. 1978;7(6):321-324. https://doi.org/10.1002/jrs.1250070606
25. Wei H, Wu M, Dong Z, et al. Composition, microstructure and SERS properties of titanium nitride thin film prepared via nitridation of sol–gel derived titania thin films. J Raman Spectrosc. 2017;48(4):578-585. https://doi.org/10.1002/jrs.5080
26. Zukalova M, Prochazka J, Bastl Z, et al. Facile conversion of electrospun TiO2 into titanium nitride/oxynitride fibers. Chem Mater. 2010;22(13):4045-4055. https://doi.org/10.1021/cm100877h
27. Wang FC, Liu CH, Liu CW, Chao JH, Lin CH. Effect of pt loading order on photocatalytic activity of Pt/TiO2 nanofiber in generation of H_2 from neat ethanol. J Phys Chem C. 2009;113(31):13832-13840. https://doi.org/10.1021/jp9033535
28. Neumann O, Urban AS, Day J, Lal S, Nordlander P, Halas NJ. Solar vapor generation enabled by nanoparticles. ACS Nano. 2013;7(1):42-49. https://doi.org/10.1021/nn304948h